HEFAT2007
5th International Conference on Heat Transfer, Fluid Mechanics and Thermodynamics
Sun City, South Africa
Paper number: AM3

DISSECTING A COMPLEX SYSTEM; A COMPUTATIONAL STUDY OF FLOW BEHAVIOR IN A SINGLE-BLADE PUMP

Auvinen M.*[1], Ala-Juusela J.[1], Ilves L.[2] and Siikonen T.[1]
*Author for correspondence
[1] Department of Mechanical Engineering, Laboratory of Applied Thermodynamics,
Helsinki University of Technology, P.O. Box 4400, Fin-02015, Finland
E-mail: mikko.auvinen@tkk.fi

[2] Oy Grundfos Environmental Finland AB, P.O. Box 1036, Fin-00101, Finland
Email: lilves@grundfos.com

ABSTRACT

In this paper a computational, time-accurate analysis of a single-blade pump, whose flow system is characterized by highly oscillatory behavior, is presented. The study lays bare the immanent challenges present in applying CFD to such complex flow systems. Four time-accurate simulations with different modeling choices are completed in order to reveal the computational flow system's sensitivities to such decisions and obtain reliable performance predictions for experimental comparison. The time-accurate simulations consistently over-predicted the hydrodynamic performance according to expectations, but demonstrated strong dependency on particular CFD aspects: The strictness of the numerical convergence and the changes in the inflow and outflow configurations have a considerable effect on the system's flow behavior. Elevated levels of uncertainty also accompany the transient simulations.

INTRODUCTION

Single-blade pumps constitute a special group among pumps, featuring geometry designed to operate in waste water conditions without clogging. Their design process is complicated by the additional requirements to tolerate fluid impurities and large object penetration, which emphasizes the role of computational fluid dynamics (CFD) in realizing a hydrodynamically efficient design. However, the single-blade geometry is challenging for CFD analysis: The widely used quasi-steady method completely fails to describe the flow system, necessitating computationally intensive time-accurate analysis. To elevate the level of computational difficulty, the single-blade geometry generates a flow system, drastically dissimilar to conventional pumps, which exhibits complex behavior and strong oscillations arising from the impeller-volute interaction and the 2π-periodicity of the system.

Computational studies completed thus far have succeeded in obtaining satisfactory performance predictions [1] and vital information about the structural response of the impeller to the oscillating flow system [2]. Yet, further scrutiny has uncovered dependencies in the flow system's behavior, which require more detailed analysis. Such continued analysis is well motivated because it is of critical interest to the designer, not only to obtain reliable performance predictions, but also to understand both global and local flow behavior, as well as the uncertainty in the computational results.

This paper investigates the role of the applied boundary conditions, geometric model variations, and solution convergence in the CFD analysis of a single-blade pump. The analysis comprises four different time-accurate simulations performed with the in-house finite volume solver FINFLO. In the first two sections of this paper the theoretical background is presented, while the subsequent sections are devoted to a description of the computational models and methods as well as a brief discussion on the physical error diagnostic method used to assess the solution accuracy. Finally, the results are analyzed and compared to empirical data [3], and the subsequent conclusion are drawn.

NOMENCLATURE

D	[W/m^2], [m]	Diffusion term, characteristic diameter
E_T, E_M	[J]	Total energy, Mechanical energy
$\vec{F}_c$, $\vec{F}_v$	[-]	Inviscid and viscous flux vectors
H_{21}	[m]	Total hydrodynamic head
$\vec{Q}$	[-]	Source term vector
S	[m^2]	Surface area
T	[K], [J]	Temperature, Torque
$\vec{U}$	[-]	Vector of conservative variables
V	[m/s]	Contravariant velocity
$\dot{W}_s$	[W]	Shaft power
e	[J/kg]	Specific internal energy
g	[m/s^2]	Acceleration due to gravity
h	[J/kg]	Specific enthalpy
k	[J/kg]	Turbulent kinetic energy
$\vec{n}$	[-]	Normal vector
$\dot{m}$	[kg/s]	Mass flow rate
p	[Pa]	Pressure
q	[J/m^3]	Heat energy
$\vec{r}$	[m]	Radial distance vector
t	[s]	Time
u,v,w	[m/s]	Cartesian velocity components
w	[J/m^3]	Specific work
x, y, z	[m]	Cartesian axis direction

Special characters

Δ		Algebraic difference
Φ	[W]	Viscous dissipation
Θ	[W/m^2]	Work due to viscous stresses and heat conduction
Ω	[rad/s]	Rotational velocity of the impeller
Ψ	[m^3]	Control volume
ε	[J/kg]	Dissipation of turbulent kinetic energy
ϵ	[W]	Numerical error in energy balance
η	[%]	Efficiency
κ	[W/mK]	Thermal conductivity
μ	[Pa s]	Fluid viscosity
θ	[deg]	Impeller blade angle
ρ	[kg/m^3]	Fluid density
τ	[Pa]	Stress tensor

Subscripts

M	Mechanical
R	Radial component
T	Total value, tangential component
c	Convection term
ε	Term related to dissipation of k
k	Term related to k
t	Term related to turbulence
v	Viscous term

GOVERNING EQUATIONS

The simulation of Newtonian fluid flow is based on the numerical solution of the complete Reynolds-Averaged Navier-Stokes (RANS) equations coupled with an appropriate turbulence model. In a computational context, it is informative to present the equations in an integral vector form

$$\frac{\delta}{\delta t}\int_{\Psi}\vec{U}\,d\Psi+\oint_{\delta\Psi}(\vec{F}_c-\vec{F}_v)\,dS=\int_{\Psi}\vec{Q}\,d\Psi \tag{1}$$

where the vector $\vec{U}$ contains the conservative variables

$$\vec{U}=\left(\rho,\ \rho u,\ \rho v,\ \rho w,\ E_T,\ \rho k,\ \rho\varepsilon\right)^T \tag{2}$$

while $\vec{F}_c$ and $\vec{F}_v$ represent the inviscid and viscous flux vector terms. On the right hand side of the equation, $\vec{Q}$, contains all the source terms through which additional physics can be accounted for. Since Chien's $k-\varepsilon$ turbulence model is utilized, the equation for turbulent kinetic energy and its dissipation are presented as well. The vectors are written

$$\underbrace{\begin{bmatrix}\rho V\\ \rho uV+n_x p\\ \rho vV+n_y p\\ \rho wV+n_z p\\ (E_T+p)V\\ \rho kV\\ \rho\varepsilon V\end{bmatrix}}_{\vec{F}_c},\quad \underbrace{\begin{bmatrix}0\\ n_x\tau_{xx}+n_y\tau_{xy}+n_z\tau_{xz}\\ n_x\tau_{yx}+n_y\tau_{yy}+n_z\tau_{yz}\\ n_x\tau_{zx}+n_y\tau_{zy}+n_z\tau_{zz}\\ n_x\Theta_x+n_y\Theta_y+n_z\Theta_z\\ n_x D_{kx}+n_y D_{ky}+n_z D_{kz}\\ n_x D_{\varepsilon x}+n_y D_{\varepsilon y}+n_z D_{\varepsilon z}\end{bmatrix}}_{\vec{F}_v},\quad \underbrace{\begin{bmatrix}0\\ 0\\ 0\\ 0\\ 0\\ Q_k\\ Q_\varepsilon\end{bmatrix}}_{\vec{Q}} \tag{3}$$

where $V=\vec{n}\cdot\vec{V}$ defines the contravariant velocity and

$$\tau_{ij}=(\mu+\mu_t)\left[\frac{\partial u_j}{\partial x_i}+\frac{\partial u_i}{\partial x_j}-\frac{2}{3}\left(\nabla\cdot\vec{V}\right)\delta_{ij}\right] \tag{4}$$

the viscous stress tensor, in which the turbulent viscosity, μ_t, accounts for the effect of the Reynolds stresses according to the Boussinesq's approximation. The terms describing the work done by the viscous stresses in the conservation of total energy equation and the diffusion of turbulent quantities are written

$$\Theta_i=u_j\tau_{ij}+\kappa\frac{\partial T}{\partial x_i}$$
$$D_{ki}=\mu_k(\partial k/\partial x_i),\quad D_{\varepsilon i}=\mu_\varepsilon(\partial\varepsilon/\partial x_i) \tag{5}$$

In time-accurate analysis, the source vector contains only the turbulence model terms, which are completely described in [1].

The equation system (1) is solved with a structured multi-block approach. The convected variables are extrapolated to the cell surfaces using a third-order upwind-based (MUSCL-type) discretization, while the diffusion terms are central-differenced. In the time-accurate solutions a three-level fully implicit scheme is employed. Since the flow is incompressible, preconditioning is used to solve the pressure. The minimum velocity scale applied in the preconditioning is limited to ten times the local velocity. The maximum value is given as input and is set to ten times the averaged inlet velocity. The same velocity scale is applied in the Rhie and Chow-type damping term in order to prevent a checkerboard solution for the pressure field. Details of the solution scheme are given in [4].

PUMP PERFORMANCE

Since the theoretical framework of the hydrodynamic behavior of the pump is fully contained in the Navier-Stokes equations, the solution, which is fixed by the specific initial and boundary conditions, embodies all the information concerning the hydrodynamic performance of the pump. Thus, the relevant information on performance is obtained from the discrete solution by evaluating the terms appearing in the pump energy balance. The derivation of the desired form of the pump energy balance starts from the First Law of Thermodynamics: $dw/dt + dq/dt = d(\rho e_T)/dt$. Integrating over the entire pump volume, the equation reads

$$\int_{\forall} \frac{dw}{dt} d\forall + \int_{\forall} \frac{dq}{dt} d\forall = \int_{\forall} \frac{d(\rho e_T)}{dt} d\forall \tag{6}$$

which can be simplified by splitting the work term on the left-hand side into flow and shaft work, and combining the flow work with the right-hand side. Utilization of Gauss's law results in

$$\dot{W}_s + \dot{Q} = \int_{\forall} \frac{\partial(\rho e_T)}{\partial t} d\forall + \int_{\partial \forall} \rho V h_T dS \tag{7}$$

where specific total enthalpy has been obtained on the right-hand side. Applying this equation to the pump with adiabatic walls $(\dot{Q}=0)$ and simplifying the notation, we arrive at

$$\dot{W}_s = \dot{E}_T + \dot{m}\,(h_{T2} - h_{T1}) \tag{8}$$

where $\dot{m}$ is the mass flow rate through the system while h_{T2} and h_{T1} stand for the specific total enthalpies at the outlet and inlet of the pump, respectively. Utilizing notation Δ to indicate differences between the values at the outlet and inlet, and the definition of total pressure in incompressible flow $(p_T = p + \rho \vec{V}\cdot\vec{V}/2)$, the energy balance can be written

$$\dot{W}_s = \dot{E}_T + \dot{m}\left(\Delta e + \Delta(p_T/\rho) + \Delta k\right) \tag{9}$$

Now, it is recognized that the only mechanism that adds to the fluid's internal energy budget comes from losses due to viscosity. This contribution is broken into two components: turbulent and viscous (i.e. laminar) dissipation, identified as Φ_t and Φ_v. Furthermore, given that T is the torque applied by the impeller to the fluid, the rate of shaft work done on the system becomes $\dot{W}_s = T\,\Omega$. Thereby, with the definition of mechanical energy $E_M = \dot{m}(p_T/\rho)$, the equation reaches its final form

$$T\Omega = \dot{E}_T + \Delta E_M + \Phi_t + \Phi_v + \dot{m}\,\Delta k \tag{10}$$

The analysis of the hydrodynamic performance of the pump primarily revolves around the evaluation of the individual components of this equation.

There are also two additional convenient measures that arise from (10) that are widely used in pump performance analysis: The total hydrodynamic head

$$H_{21} = \frac{\Delta p_T}{\rho g} = \frac{\Delta E_M}{\dot{m} g} \tag{11}$$

and the hydrodynamic efficiency of the pump

$$\eta = \frac{\Delta E_M}{T\,\Omega} \tag{12}$$

It should be noted, however, that experimental measurements typically indicate the total (or shaft) efficiency of the system, which includes the associated bearing and shield losses.

PUMP GEOMETRY AND COMPUTATIONAL MODELS

The investigated single-blade pump design, which is often referred to as a single-channel design, features a shrouded impeller with an integrated blade that has a wrap angle of 360 degrees and an exit angle of 6 degrees relative to the tangential direction. The system has a free passage diameter of 80 mm. See Figure 1 for an overview.

The computational grid models were generated utilizing the complete CAD geometry with the following modification: The impeller shroud diameter was extended by 10% to cover the tip of the blade, which would otherwise have protruded into the domain of the volute. This alteration enabled structured grid generation and time-accurate sliding plane analysis. The overall geometric complexity of the pump rendered structured grid generation demanding (see Figure 2) and the model prone to grid quality deficiencies.

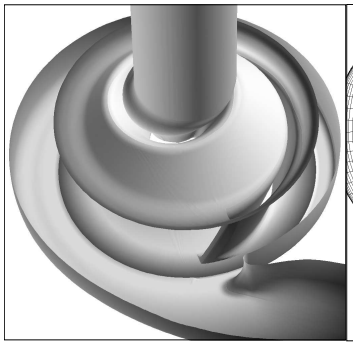

Figure 1: An overview of the pump geometry.

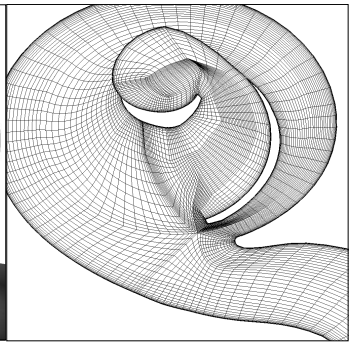

Figure 2: A central bisecting grid plane. Shown blade angle θ=0 deg.

Constant diameter sections of the intake and exit ducts were included in the initial computational model, labeled *A* in Figure 3, to allow attenuation of disturbances in the flow field and to ensure that the imposed inlet and outlet boundary conditions do not restrict the flow unrealistically. However, the highly fluctuating nature of the flow system necessitated further examination of such modeling choices. Thus an alternate model was constructed in an attempt to reduce the effect of the imposed boundary conditions. This model, labeled *B* in Figure 4,

features tank-like intake and exit ducts to guarantee placid conditions at the inlet and outlet boundaries.

The structured multi-block grids employed in this study consist of 275,000 (*A*) and 315,000 (*B*) cells with an average $y^+ \approx 5$. Since increasing the cell count of model *A* to *2.2* million ($y^+ \approx 2$) resulted in a maximum deviation of 3% in performance predictions, the utilized grids were deemed sufficient for this computationally heavy investigation.

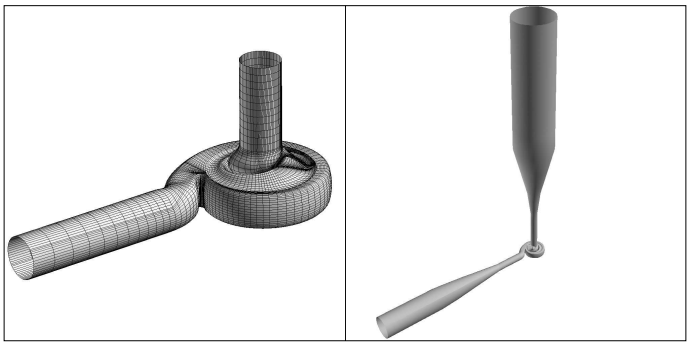

Figure 3: Overview of model *A*. **Figure 4:** Overview of model *B*.

CFD ANALYSIS

The objective of this numerical analysis was to replicate the conditions present at an experiment conducted by the manufacturer [3] in order to obtain comparable performance predictions and flow behavior. Four time-accurate simulations with different geometric configurations or boundary conditions are completed in order to evaluate the sensitivity of the flow system to such variations. The baseline boundary conditions for the pump are provided in Table 1. All surfaces adhere to the no-slip condition and $\vec{u}_{wall} = \vec{\Omega} \times \vec{r}$ defines the impeller wall velocity.

Table 1: Applied boundary conditions

Boundary Condition	*Value*
Inlet: Mass flow rate	$\dot{m} / (\rho \Omega D^3) = 0.223$
Inlet: Fluid temperature	$T_{inlet} = 293.15$ K
Outlet: Reference Pressure	$p_{outlet} = 8.0 \times 10^5$ Pa
Impeller: Rotational Velocity	$\lvert\Omega\rvert = 151.63\, s^{-1} = 1448$ RPM

The different cases, listed in Table 2, were selected in order to highlight central dependencies, which must be accounted for in the time-accurate analysis of such systems. The first two cases, *A1* and *A2*, feature identical grid models (*A*) and boundary conditions, but differ in the number of inner iterations, i.e. in the level of convergence within a time-step. The third case, *A3*, while also employing grid *A*, utilizes alternative boundary conditions: a constant pressure condition at the inlet and a constant $\dot{m}$ condition at the outlet. Such boundary condition treatment, while lacking physical justification, has traditionally been utilized in CFD analysis of pumps due to the improvement in numerical stability. Nonetheless, since the constant $\dot{m}$ inlet boundary condition is questionable for this system, this alternative deserves to be considered. The final case, *B*, attempts to diminish the effect of the inlet and outlet conditions by introducing tank-like intake and exit ducts, which allow the system to fluctuate with increased freedom.

Table 2: Description of the computational cases.

Label	*Definition*
A1:	Iterations per time-step: Iter = 400
A2:	Iterations per time-step: Iter = 135
A3:	Inlet BC: Pressure, Outlet BC: Velocity. Iter = 215
B :	Extended model. Iter = 215

With all the cases the time derivative was evaluated with a three-level second order accurate explicit discretization scheme and the physical time-step, Δt, was defined such that $\Delta\theta = \Omega \Delta t = 1.0$ deg. A second order accuracy in time was found necessary to resolve the multi-modal oscillations in the flow system.

Error Diagnostics

The impracticality of applying the Richardson extrapolation method to complicated industrial applications calls for alternative methods for error assessment. A physical error diagnostic method [5] which utilizes the expression for the global energy balance (10) has proven highly convenient and informative in this study. The basic idea of physical error diagnostics is to test the validity of the obtained discretized solution with physical constraints which are not explicitly enforced by the numerical solution scheme. If the method is consistent and the discretization error small, the solution should satisfy these conditions.

The global energy balance method is based on quantifying the violation in the energy equation (10), which is basically a rewritten expression of the conservation of total energy. A measure of such error ϵ can be evaluated from

$$T\Omega - \left(\dot{E}_T + \Delta E_M + \Phi_t + \Phi_v + \dot{m}\, \Delta k \right) = \epsilon \qquad (13)$$

which contains all the terms in the pump energy budget. Although it has been shown that in quasi-steady analysis ϵ diminishes with increasing grid density and quality, the method may not yield conclusive information about the solution accuracy. However, it does lay bare a concealed problem in RANS analysis: Despite numerical convergence, the obtained physical measures may not comply with all conservation requirements. This problem becomes particularly discernible in the time-accurate analysis of highly oscillatory systems and, therefore, it demands appropriate attention.

RESULTS

All the time-accurate simulations were ran until the system had settled into a periodic pattern, making the analysis computationally intensive. If the simulation was restarted from a quasi-steady solution, this required approximately 8 revolutions with model *A* and up to 16 revolutions with model *B*. To assure comparability, the head and efficiency measurements of both models were extracted from the same inlet and outlet planes.

The computational performance measures, which are averaged over one revolution, are compared to the empirical measurements in Table 3. These results lead to the following three deductions. First: The general outcome is favorable because all simulations over-estimated the hydrodynamic efficiency and head according to expectations, since the empirical values embody additional shield and bearing losses. Second: Regardless of the right trend, the analysis yielded a high margin of uncertainty due to the system's elevated sensitivity to the level of convergence within a time-step (*A1* vs. *A2*) and to the geometric modeling choices (*A* vs. *B*). The fact that all the cases reached a steady periodic behavior evidently does not provide any guarantee that the solutions are physically sound. Third: Imposing a constant $\dot{m}$ boundary condition at the outlet alters the mean results in efficiency, but reaches close agreement in $T\Omega$ and H_{21} with the thoroughly converged case *A1*.

Table 3: Empirical and computational results

	Shaft Power (scaled) $T\Omega/\rho\Omega^3D^5$ $\left(\times10^{-2}\right)$	Head (scaled) H_{21}/Ω^2D^2 $\left(\times10^{-2}\right)$	Efficiency η (%)
Emp:	*16.28*	*5.39*	*71.1*
A1:	*15.44*	*5.53*	*78.6*
A2:	*16.62*	*5.87*	*77.6*
A3:	*15.54*	*5.52*	*75.9*
B:	*15.96*	*5.48*	*76.0*

Although the mean results are informative and important, they completely conceal the time-dependent behavior of the system, which is crucial for the designer, for instance, in predicting the resulting hydrodynamic excitation forces exerted on the structures. The simulated flow system of the pump ends up being characterized by exceptionally strong impeller-volute interaction, which gave rise to intense pressure oscillations in the flow field. This dramatically oscillating nature of the pump becomes apparent from the time-accurate data in Figures 5 – 7. Consequently, the oscillating behavior proves computationally problematic: The pressure fluctuations affect the flow at both inlet and outlet boundaries and, since the velocity field is fixed at one end, the pulsating mass flux in the other results in a violation of the conservation of mass. This emerging compressible behavior further enhances the oscillations, particularly with model *A*, and manifests itself as excessive highs and lows in hydrodynamic head and efficiency. The extended model *B* successfully dampens the behavior, but comes at a heavy computational cost.

As shown in Figure 5, the impeller-volute interaction is most pronounced when the tip of the blade meets the tongue of the volute (θ = 0 deg, shown in Figure 2). This resulting peak in shaft power requirement is so forceful that it renders the coupled fluid-structure interaction significant. Because such an analysis would be impractical for design purposes, alternative methods should be investigated as well. For instance, by assigning a realistic rotational inertia to the impeller-motor system, the constant Ω assumption could be replaced by $\Omega(T)$. Before such studies are launched, however, the CFD-related uncertainties must be reduced and the modeling sensitivities understood.

Inspection of Figures 6 and 7 reveals how the modality of the pressure oscillations depend on both inner convergence (*A1* vs. *A2*) and the flow boundary conditions (*A1, B* vs. *A3*). The agreement between A1 and B suggests that they have captured the pump's natural mode, but there is no experimental data for validation.

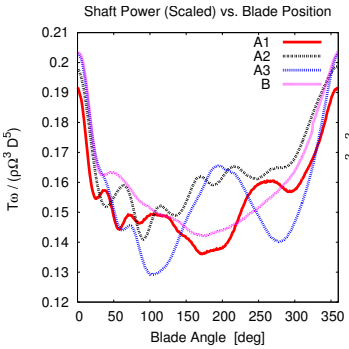

Figure 5. Transient behavior of shaft power requirement ($T\Omega$).

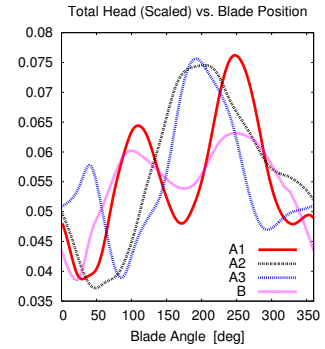

Figure 6. Transient behavior of hydrodynamic head (H_{21}).

Although time-accurate data on the global energy balance error is not available at this stage, the periodical monitoring of this quantity has indicated that the error fluctuates considerably between positive and negative values, following the modality of the system. While it seems that the time-averaged error does not amount to much, the magnitudes of the peak values are regretfully high. Utilizing the error obtained from a quasi-steady case as a reference ($\epsilon_{qs}=0.047\ T\Omega$), the time-accurate cases yielded as high as $max(|\epsilon(t)|)\approx5\epsilon_{qs}$. The peak error values did decline with better convergence (*A1*) and subdued oscillations (*B*), but not drastically. Therefore, in order to reduce the uncertainty of the transient solutions, it is critical to devote further attention to this issue and investigate what kind of role the numerical solution method plays in this matter.

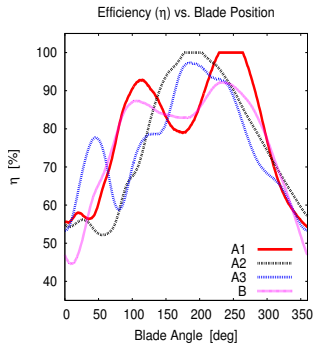

Figure 7. Transient behavior of pump efficiency (η).

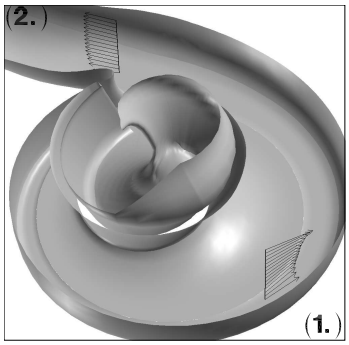

Figure 8. The locations of the velocity profile measurements.

In order to gain greater insight into the flow behavior in the pump, empirical velocity profile measurements were obtained through Laser Doppler Velocimetry (LDV) at the locations shown in Figure 8. Both radial and tangential velocity profiles were measured at every blade angle (360) within a revolution. Such data has enabled time-accurate comparisons between empirical and computational measurements to be prepared. These animations have proven remarkably helpful in unveiling the complexity of the flow field and in assessing the validity of the computational results. Although the complete picture cannot be drawn without the animations, a single frame shown in Figure 9 succeeds in describing the overall situation: At location 1, where the blade-volute interaction dominates the flow behavior, the comparison yields striking agreements especially in the dominant tangential direction. However, it is the radial profile that warrants closer inspection, since in this region it is of particular interest to the designer. Both empirical and computational profiles exhibit inward flow at the center of the channel, which is evidence of the significant role played by the continuous disc pumping effect of the hub and the shroud, which manifests as pronounced radial outflow at each end. However, the empirical profile displays greater vorticity, which is not captured by the RANS simulations, in part due to the simplifications in the model geometry.

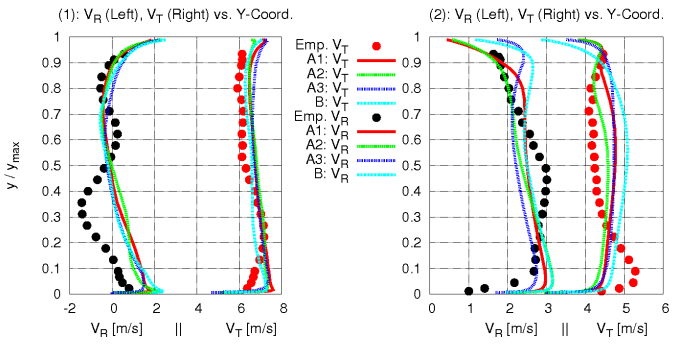

Figure 9. Empirical and computational velocity profiles at two different locations in the volute.

The velocity profiles at location 2 are no longer dominated by the impeller-volute interaction and thereby reveal greater differences between computational cases. Nonetheless, the general agreement with the empirical measurements remains satisfactory.

CONCLUSIONS

The performed computational study of a single-blade pump led to the following conclusions:

- While the time-accurate CFD results yield favorable performance predictions, they also depict pronounced sensitivities to the different modeling choices.
- The highly oscillating flow behavior proved computationally problematic: Sufficient convergence within a time-step is necessary to capture the oscillating behavior correctly. Also, the pressure field has a tendency to exhibit excessive highs and lows, except in the case of the expanded model configuration.
- The comparison between computational and empirical velocity profile data demonstrates marked agreements, although the empirical radial velocity profiles near the blade depict greater vorticity than the RANS model, which contains simplifications in the impeller geometry.
- The utilized physical error diagnostic method revealed that the time-accurate CFD simulations were associated with high levels of energy balance violations. However, the behavior of the error fluctuates according to the flow field, which confines the accumulated error. This issue calls for further investigation.

REFERENCES

[1] Auvinen, M., Ala-Juusela, J., Siikonen, T., "CFD Modeling of a Sing-Blade Pump," in *Proceedings of the IX Finnish Mechanics Days, Lappeenranta,* Vol. 1, pp. 167-179, June 2006.

[2] Benra, F.-K., "Numerical and Experimental Investigation on the Flow Induced Oscillations of a Single-Blade Pump Impeller," *Journal of Fluids Engineering,* Vol. 128, pp. 783-793, July 2006.

[3] Pedersen, N., Sorensen, H., "Flow Investigation in a Single-Channel Pump Using LDV," in *Conference on Modelling Fluid Flow (CMFF'03), (Budapest, Hungary), The 12th International Conference on Fluid Flow Technologies*, September 1997.

[4] Rahman, M., Rautaheimo, P. and Siikonen, T., "Numerical Study of Turbulent Heat Transfer from a Confined Impinging Jet Using a Pseudo-compressibility Method," in *Proceedings of the 2nd International Symposium on Turbulence, Heat and Mass Transfer, (Delft)*, pp. 511-520, June 1997.

[5] Haworth, D., El Tahry, S. and Huebler, M., "Global Approach to Error Estimation and Physical Diagnostics in Multidimensional Computational Fluid Dynamics," *International Journal for Numerical Methods in Fluids*, Vol. 17, 1993, pp. 75-97.